Oceanologia (2021) 63, 238—246

Available online at www.sciencedirect.com

ScienceDirect

journal homepage: www.journals.elsevier.com/oceanologia

ORIGINAL RESEARCH ARTICLE

Lidar observation of aerosol transformation in the atmospheric boundary layer above the Baltic Sea

Przemysław Makuch[a,*], Stefan Sitarek[b], Piotr Markuszewski[a,c,d], Tomasz Petelski[a], Tadeusz Stacewicz[e]

[a] *Institute of Oceanology, Polish Academy of Sciences, Sopot, Poland*
[b] *Institute of Applied Optics, Warsaw, Poland*
[c] *Department of Environmental Science, Stockholm University, Stockholm, Sweden*
[d] *Bolin Centre for Climate Research, Stockholm University, Stockholm, Sweden*
[e] *Institute of Experimental Physics, University of Warsaw, Warsaw, Poland*

Received 22 April 2020; accepted 29 January 2021
Available online 9 February 2021

KEYWORDS
Aerosol;
Lidars measurements;
Atmospheric boundary layer

Abstract Investigation results of a coarse and accumulation mode of aerosol properties above the Baltic Sea are reported. A most important role in the direct aerosol effect on climate have aerosols from the group of coarse and accumulation mode particles. Overseas in the atmosphere, there is a lot of aerosols from the fine fraction but their impact is not so important as coarse and accumulation mode particles. Sea spray emission from the sea surface takes place over a wide range of aerosol particle size distribution, it is also large in size range which are studying in this work (Lewis and Schwartz, 2004). The discussed range is most important in view of atmospheric optical properties, smaller particles do not have such an influence on scattering as particles from range 0.5—2 μm. The research was performed with a multiwavelength lidar. Due to the application of special software, the aerosol particle size distributions were retrieved from the lidar returns. That provided an opportunity to determine the profiles of the aerosol effective radius. We showed that the aerosol properties depend mainly on the direction of the air mass advection and the wind speed. The impact of the Baltic Sea on the aerosol size distribution is huge in the case of the advection from the open sea. Moreover, the aerosol effective radiuses in the whole boundary layer are much larger in the case of strong than for light wind.

* Corresponding author at: Institute of Oceanology, Polish Academy of Sciences, Powstańców Warszawy 55, 81—712 Sopot, Poland.
E-mail address: makuch@iopan.pl (P. Makuch).
Peer review under the responsibility of the Institute of Oceanology of the Polish Academy of Sciences.

Production and hosting by Elsevier

https://doi.org/10.1016/j.oceano.2021.01.002

Our results suggest that the aerosol flux and the aerosol particle size distribution should be related to the wind speed in the emission function.

1. Introduction

Atmospheric aerosol plays an especially important role in the climate system. It significantly influences the amount of solar energy that is supplied to the earth's surface (Forster et al., 2007). The overall impact of aerosol on energy transfer through the atmosphere, called the aerosol effect, operates through direct and indirect mechanisms. The first one takes place due to sun's energy extinction by the aerosol, the second consists of aerosol influence on clouds in the atmosphere (Lohmann and Feichter, 2005; Stevens and Feingold, 2009; Streets et al., 2006; Tao et al., 2012; Twomey, 1977; Wood et al., 2015). Therefore, the determination of aerosol properties and their evolution under various atmospheric conditions are hugely important scientific challenges.

Transformation of the aerosol contained in air masses transported over large water surfaces, such as oceans, seas and huge lakes, is a well-known phenomenon (Plauškaitė et al., 2017; Zdun et al., 2016). Various processes are responsible for such an effect. Sea spray emission from the water surface and prolapse of aerosol particles from the atmosphere are the most important ones. Along the path of the air masses, the scavenging of the aerosol to the constituent typical for marine aerosol is observed (Blanchard, 1954; Cipriano et al., 1983; Resch et al., 1986; Spiel, 1994, 1995, 1997a, 1997b, 1998). Phenomena such as change of air masses, humidity and nucleation of secondary aerosol from the gasses present in the atmosphere are of huge importance as well.

The properties of the aerosol over the Baltic Sea surface strongly depend on the features of the air masses advecting from various directions (Lewandowska and Falkowska, 2013a, 2013b; Nadstazik et al., 2000; Zdun et al., 2011). Therefore, the Baltic aerosol can be of significantly different properties and chemical compositions. Insofar as these features are also determined by the aerosol origin, its transport over the sea surface can strongly influence its physical and chemical properties. This takes place mainly because of the aerosol emission from the sea surface to the atmospheric boundary layer, which causes the increase of the effective particle radius (Lewis and Schwartz, 2004). Particle deposition on the sea surface and scavenging of continental aerosol by marine particles are another important processes changing the effective particle radius.

These processes have already been investigated by several authors in various locations at the Baltic seashore (Kikas et al., 2008; Kuśmierczyk-Michulec, 2009; Kuśmierczyk-Michulec and Marks, 2000; Kuśmierczyk-Michulec and Rozwadowska, 1999; Zdun et al., 2011). Zieliński (2004) showed that the aerosol parameters in coastal regions depend on the wind direction (overland and maritime), which confirms the huge emission of the aerosol from the Baltic surface. The flux of the marine aerosols emission in the coastal range of the south Baltic was determined and parametrised using waves energy by Petelski and Chomka (1996, 2000) and Chomka and Petelski (1997). The aerosol emission on the open Baltic Sea was investigated as well (Markuszewski et al., 2020; Massel, 2007; Petelski, 2003; Petelski et al., 2005).

The aim of this work was to confirm the phenomenon of the aerosol changes over the Baltic surface using lidar for determination of aerosol particle sizes.

2. Material and methods

A measurement campaign was performed in January and February 2015. The lidar system was installed in Władysławowo (54.803N, 18.396E), Poland, about 50 metres away from the coastline. Such a location is convenient because of the winds occurring there. In the case of their westerly direction blowing along the seashore, one can observe the aerosol that is not converted by the water area. In the case of northerly winds, one registered the air masses that were transported for hundreds of kilometres above the Baltic surface.

A 3-wavelength lidar was applied in this experiment (Posyniak et al., 2010, 2011). A pulsed Nd:YAG laser (Brilliant, Quantel) was used in the optical transmitter. The laser-generated light pulses at wavelengths of 1064, 532 and 355 nm with energies of 100, 60 and 40 mJ, respectively. FWHM duration of the pulses was 6 ns, while their repetition rate was 10 Hz. A Cassegrain telescope with a 150 mm mirror was used in the optical receiver. The lidar overlap reached an altitude of approximately 850 m (Stelmaszczyk et al., 2005). In order to investigate the aerosol at low altitudes (starting from 200 m) the laser beam was sent towards the sea at an angle of 13° with respect to the horizontal plane.

Lidar operating at several wavelengths provides an opportunity to determine profiles of size distribution of atmospheric aerosol particles. Our approach to this problem has already been presented in several papers (Jagodnicka et al., 2009; Sitarek et al., 2016). Briefly, in our experiment, the return light pulses collected by the telescope were spectrally separated by a polychromator and registered in the channels corresponding to the consecutive wavelengths (Chudzyński et al., 2004). The signals from the photomultipliers installed in each channel were digitised by 12-bit, 50 MHz A/D converters (Tie Pie Handyscope HS4). In order to increase the signal to noise ratio, the data were averaged over 30 min time intervals and then smoothed over the altitude intervals of 30 m.

As a consequence, the lidar provided the set of the distance-dependent (z = distance) signals $S_1(z)$, $S_2(z)$, $S_3(z)$

corresponding to consecutive wavelengths λ ($\lambda = 1, 2, 3$):

$$S_\lambda(z) = \frac{A_\lambda \beta_\lambda(z)}{(z - z_0)^2} \exp\left(-2 \int_{z_0}^{z} \alpha_\lambda(y) dy\right) \quad (1)$$

here, z_0 denotes the lidar position, A_λ are the wavelength-dependent apparatus constants, while $\alpha_\lambda(z)$ and $\beta_\lambda(z)$ denote the spatial distribution of total atmospheric extinction and backscattering coefficients, respectively. Range corrected signals, which are more useful for the analysis, take the form:

$$L_\lambda(z) = A_\lambda \beta_\lambda \exp\left(-2 \int_{z_0}^{z} \alpha_\lambda(y) dy\right) \quad (2)$$

The coefficients of total atmospheric extinction and backscattering (α_λ and β_λ, respectively) can be expressed as a sum of constituents (Seinfeld and Pandis, 1997):

$$\alpha_\lambda(z) = \alpha_{R\lambda}(z) + \alpha_{A\lambda}(z) = \alpha_{R\lambda}(z) + \int_0^\infty Q_\lambda^E(r) \pi r^2 n(z, r) dr \quad (3)$$

$$\beta_\lambda(z) = \beta_{R\lambda}(z) + \beta_{A\lambda}(z) = \beta_{R\lambda}(z) + \int_0^\infty Q_\lambda^B(r) \pi r^2 n(z, r) dr \quad (4)$$

The coefficients $\alpha_{R\lambda}$ and $\beta_{R\lambda}$ corresponding to Rayleigh scattering were evaluated using the approach of Bodhaine et al. (1999), assuming the standard atmosphere profiles. Aerosol scattering coefficients ($\alpha_{A\lambda}$ and $\beta_{A\lambda}$), described by relevant integrals, were evaluated by Mie theory Bohren and Huffmann, 2010). A spherical shape of the particles was assumed. Therefore, r denotes the particle radius in the Equations (3) and ((4), and $Q_\lambda{}^E$ and $Q_\lambda{}^B$ are extinction and backscattering efficiencies, respectively. Function $n(z,r)$ describes distance-dependent aerosol particle size distribution (APSD), which is the matter of this investigation.

The lidar returns provided by the apparatus were quantised in space, with the interval Δz resulting from the digitisation rate and smoothing procedure. Therefore, at a distance z_l for each wavelength, the signals (2) can be expressed by:

$$L_\lambda(z_l) = A_\lambda \beta_\lambda(z_l) \exp\left\{-\Delta z \sum_{i=2}^{l} [\alpha_\lambda(z_{i-1}) + \alpha_\lambda(z_i)]\right\} \quad (5)$$

Here the integral from Eq. (2) was approximated by use of the trapezoidal approach. For further analysis, the ratio of the signals at the distances z_l and $z_{l+1} = z_l + \Delta z$ was taken:

$$\frac{L_\lambda(z_{l+1})}{L_\lambda(z_l)} = \frac{\beta_\lambda(z_{l+1})}{\beta_\lambda(z_l)} \exp\{-\Delta z[\alpha_\lambda(z_l) + \alpha_\lambda(z_{l+1})]\} \quad (6)$$

This allowed omitting the apparatus constants A_λ, which were unknown.

The left-hand side of Eq. (6) describes the ratio of the experimental signals. The extinction and backscattering coefficients in Eqs. (3) and (4) were substituted to the right side of the equations.

In our approach, $n(z,r)$ in a predefined form of two-mode function, Eq. (7), was derived:

$$n(z, r) = \sum_{j=1}^{2} n_j(z, r) \quad (7)$$

where each mode was described by a log-normal function:

$$n_j(z, r) = \frac{C_j}{\sqrt{2\pi} \cdot \log\sigma_j(z)} \cdot \frac{1}{r} \cdot \exp\left\{-\frac{[\log r - \log R_j(z)]^2}{2 \cdot \log^2 \sigma_j(z)}\right\} \quad (8)$$

Here, R_j, C_j and σ_j are free parameters and denote the modal radius, the amplitude and the mode width, respectively.

Our approach to retrieving APSD consists of direct substitution of α_λ and β_λ coefficients from Eqs. (3) and (4) to Eqs. (7) and (8) (Jagodnicka et al., 2009; Sitarek et al., 2016). As a result, only one unknown function (i.e. APSD) remains in Eq. (8) because both coefficients depend on the aerosol distribution. It is determined by the set of free parameters mentioned above. In order to find their values, we constructed a cost function:

$$\chi^2 = \sum_{\lambda=1}^{3} \left(\frac{L_\lambda(z_{l+1})}{L_\lambda(z_l)} - \frac{\beta_{R\lambda}(z_{l+1}) + \int_0^\infty \pi r^2 Q_\lambda^B(z_{l+1}) n(r, z_{l+1}) dr}{\beta_{R\lambda}(z_l) + \int_0^\infty \pi r^2 Q_\lambda^B(z_l) n(r, z_l) dr} \times \exp\left\{-\Delta z \begin{bmatrix} \alpha_{R\lambda}(z_l) + \\ +\alpha_{R\lambda}(z_{l+1}) + \int_0^\infty \pi r^2 Q_\lambda^E(z_l) n(r, z_l) dr \\ + \int_0^\infty \pi r^2 Q_\lambda^E(z_{l+1}) n(r, z_{l+1}) dr \end{bmatrix}\right\}\right) \quad (9)$$

The function $n^{\min}(r,z)$ with the set of the parameters that correspond to minimal value of the cost function, Eq. (9), should be accepted as the solution. However, the bimodal lognormal function found by such minimisation procedure is not unique. Quite satisfactory results (i.e., the comparable values of the χ^2 parameter) were achieved for several different $\{C_1, R_1, \sigma_1, C_2, R_2, \sigma_2\}$ sets. Therefore, a group of 300 of the results with smallest χ^2 was chosen. The values of χ_i^2 ($i = 1 \div 300$) for each set of such parameters did not differ by more than about several tens of percent.

Bimodal lognormal function $n_i^{\min}(r, z)$ was generated for each set of such parameters. As a final result of APSD retrieval, the weighted average of these functions was accepted.

$$n_{opt}(r, z) = \frac{\sum_{i=1}^{300} \chi_i^{-2} n_i^{\min}(r, z)}{\sum_{i=1}^{300} \chi_i^{-2}} \quad (10)$$

The values of χ_i^{-2} were taken as weights for this averaging.

Finally, this APSD function was used for calculation of the effective radius of aerosol particles using the formula

$$r_{eff}(z) = \frac{\int r^3 n_{opt}(r, z) dr}{\int r^2 n_{opt}(r, z) dr} \quad (11)$$

Determination of uncertainty of the method requires a numerical experiment. Such analysis was performed by Jagodnicka et al. (2009). The relative error of the approach was evaluated for 50%.

3. Results

Within all campaigns, the useful data were registered on February 7, 8, 9 and 19 only. We present these data in Figures 1 and 2. The data were averaged over 30 min, i.e.

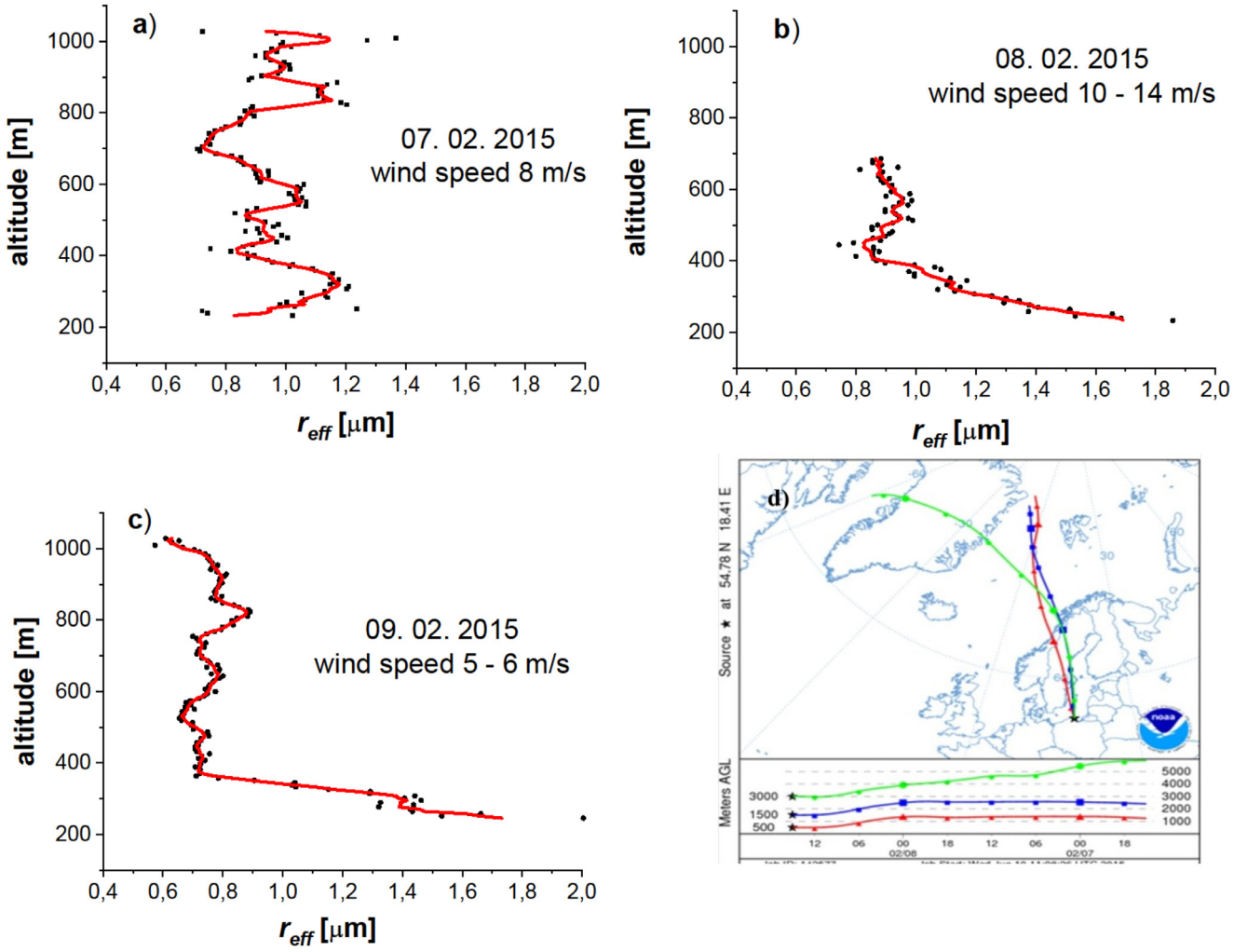

Figure 1 Vertical profiles of aerosol effective radius registered within February 7—9 (a—c) and corresponding backward trajectories of the air masses (d).

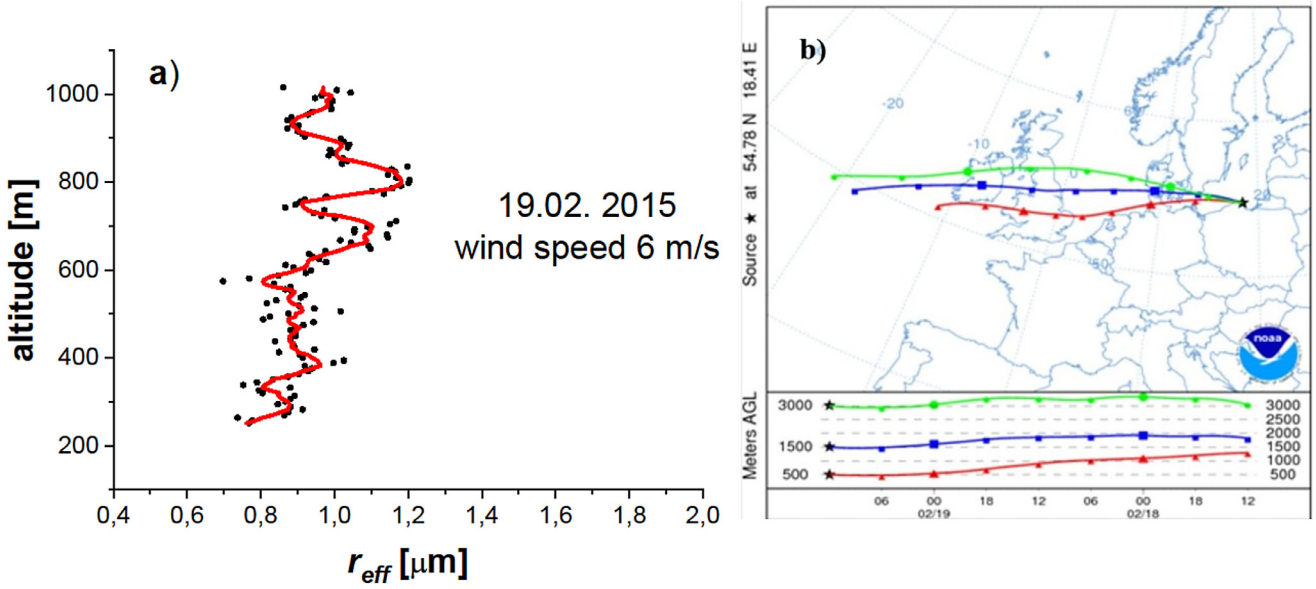

Figure 2 Vertical profile of aerosol effective radius registered on 19 February (a) and corresponding backward trajectories of the air masses (b).

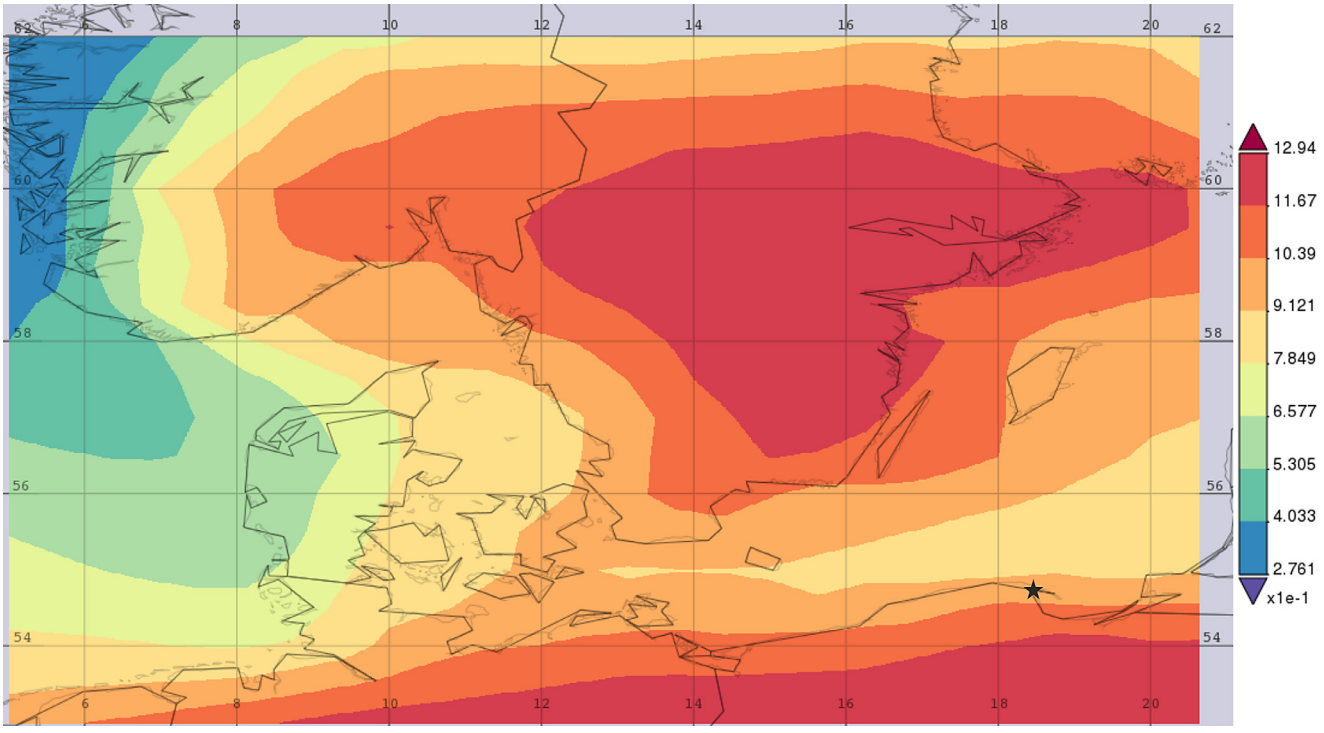

Figure 3 Map of Total Aerosol Ångstrom parameter (470—870 nm), 2015-02-07 01Z through 2015-02-07 12Z.

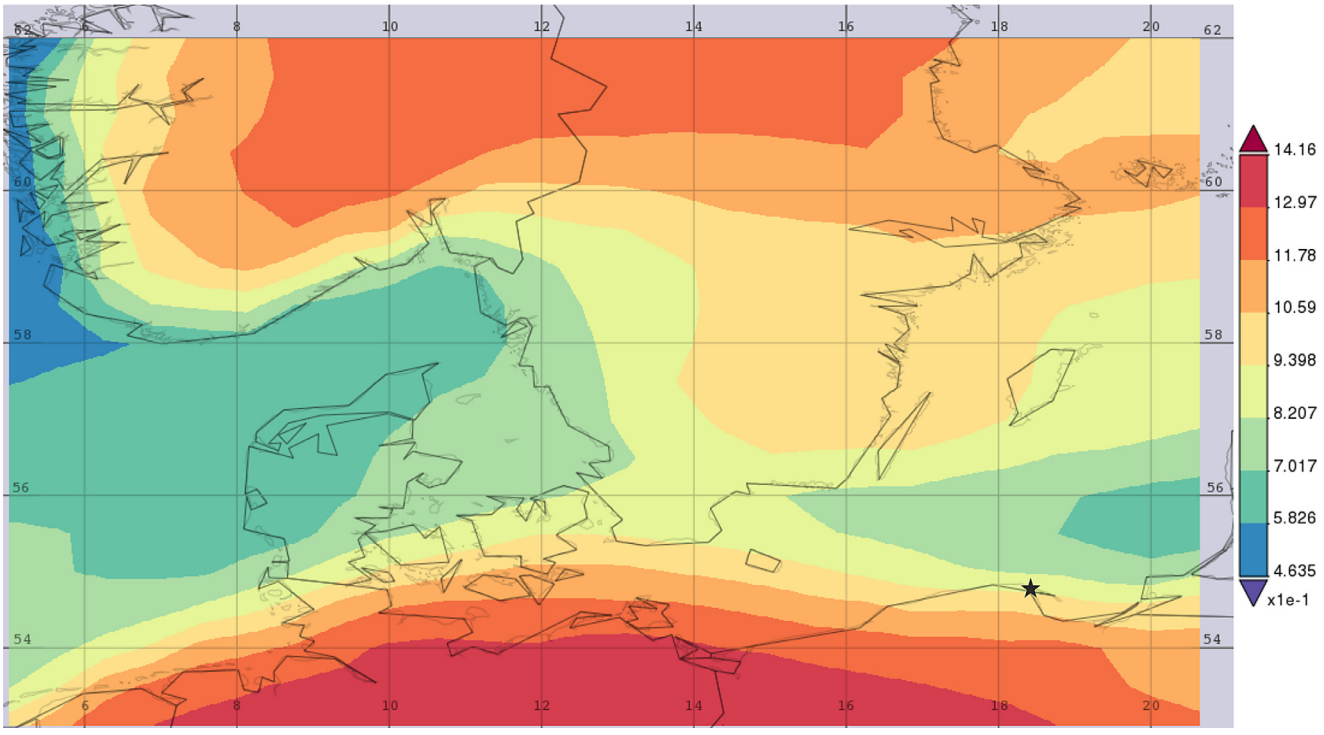

Figure 4 Map of Total Aerosol Ångstrom parameter (470—870 nm), 2015-02-19 01Z through 2015-02-19 12Z.

over 18 000 laser shots. Altitude resolution of data registration was 7 m (dots in the figures). Continuous red lines correspond to the smoothing of the results by adjacent averaging over 5 points (i.e. 35 m). Detailed analysis of the backward trajectories of the air masses within these days as performed with the HYSPLIT model (Draxler and Rolph, 2010) are also shown in these figures.

On February 7—9 the advection occurred from the north, from the open sea (Figure 1). On 7 February the wind speed increased from 8 m/s (5B on the Beaufort scale), reaching

10–14 m/s (6B) the next day, then it decreased to 5–6 m/s (3B) on the next day. Regarding February 19 (Figure 2), the advection took place from the western Baltic. The wind direction at 10 m above the surface at the experimental point was NW and W, with a speed of 6 m/s (3B).

In the case of the strong wind with speed 10–14 m/s (6B, 8 Feb., Figure 1b), one observes a monotonic decrease of the effective radius from about 1.8 μm at an altitude of 250 m to approximately 0.8 μm at 450 m. This was probably caused by an emission of coarse aerosol particles from the sea surface covered by spume. Next day (9 February), the wind speed was 5–6 m/s only (3B, Figure 1c). Under such circumstances, the spume on the waves is very weak. Nevertheless, such a monotonic character of the particle size distribution was also observed, but this layer reached lower altitudes (about 250–370 m), and the aerosol effective radiuses were smaller: 1.7–0.7 μm. This layer could be the residual effect from the previous day.

One does not observe the layer of larger particles with monotonic distribution on 7 and 19 February. Such behaviour of the effective radius extends from lower altitudes (200 m) to the maximum of the lidar range (1000 m). The variation of the effective radius occurs within 0.7–1.2 μm range. This is caused by a weak emission from the sea surface, arising from its weak covering by a spume at low wind speeds. In both cases, the wind force in the preceding days was 3B and less, so the aerosol production from the sea surface was negligible. Although on 7 February the wind speed (8 m/s) was higher than on February 9 (5–6 m/s), nonetheless on 7 February aerosol production was not observed. However, two days later, with the weaker wind, the aerosol generated on February 8 remained, as was mentioned above.

Our interpretation is confirmed by the analysis of the Ångstrom parameter spatial distribution. We used the data from the Global Modeling and Assimilation Office (GMAO, 2015). Data presented in Figures 3–5 come from MERRA-2 Model M2T1NXAER v5.12.4 and it is time-averaged hourly with 0.5 × 0.625 deg resolution. On 7 and 19 February the Ångstrom parameter did not change along the trajectory path of the air masses (Figures 3 and 4). Within the majority of the path its values were close to 1.0 and 0.7–0.8 on February 7 and 19, respectively. A different situation is seen on February 8 and 9 (Figure 5). On 8.02 at lidar position the Ångstrom parameter was close to 0.1, while for the air masses located before the measurement area its value was about 0.4–0.5. On 9 February, this effect was also seen; the difference was about 0.3. One can relate it to the emission of large aerosol particles from the sea surface. Their appearance in the atmosphere led to a decrease in the Ångstrom coefficient. These cases show how aerosols from the Baltic Sea can be transformed in the atmospheric boundary layer.

4. Discussion

In order to verify aerosol production from sea surface spray, generation functions (SSGF) were investigated. A wide variety of such functions is presented in the literature (de Leeuw et al., 2011). We compared three of them which were elaborated using micrometeorological methods. Two of them (Norris et al., 2012; Ovadnevaite et al., 2014) were built for the open ocean region, using an eddy covariance approach. The third one was elaborated using the so-called gradient method (Petelski, 2003), conducted on board a scientific vessel in the southern Baltic Sea (Petelski et al., 2014).

In order to obtain theoretical effective radiuses using SSGFs, the aerosol distributions estimated by this function were substituted into Eq. (11). Each integral was calculated for the corresponding size range in which the functions were defined. Results of the comparison are presented in Figure 6.

In the case of marine advection, the measurements are in good agreement with theoretical predictions that prove a strong influence of sea spray on the effective radius in the boundary layer. Only the function of Ovadnevaite et al. (2014) predicts a rise of r_{eff} with an increase in wind speed, but a very weak one. Effective radiuses determined using the function by Petelski (2003) (which was found on the basis of the measurements in the Baltic Sea) predicts no change, while the values estimated by means of Norris et al. (2012) functions decrease with wind speed increase. In the case of the western advection, we do not observe an influence of sea spray on the effective radius.

The variability of estimated radiuses follows from the properties of each function. The functions of Petelski (2003) and Norris et al. (2012) are the results of rough polynomial fitting in a logarithmic space. The function of Ovadnevaite et al. (2014), however, is based on multilognormal size distribution for a wide size range of particles and it is in good agreement with our observations.

It is in agreement with the newest theoretical function of Ovadnevaite et al. (2014). At the same time, our measurements show that the functions should be more dependent on wind, as is clearly visible in Figure 6.

5. Conclusions

Profiles of APSD registered with a multiwavelength lidar have been used for calculation of altitude dependent aerosol particle effective radius. It was found that these radiuses were generally larger in the case of the strong winds. For the wind from the open sea a monotonic decrease of the effective radius from about 1.8 μm at an altitude of 250 m to approximately 0.8 μm at 450 m was observed. This was probably caused by an emission of coarse aerosol particles from the sea surface covered by spume.

Our results suggest that a change of commonly used sea spray generation functions (SSGF) should be performed. Majority of them does not include the dependence of APSD on the wind speed. Such a relation is taken into account for the particles flux only. Petelski et al. (2005) postulated that both quantities, i.e. the aerosol flux and the APSD, should be related to the wind speed in the emission function. We found that otherwise the effective radius does not change or even decreases with the wind speed increase (as shown in Figure 6), when these functions are applied to Eq. (11). This is inconsistent with our observations.

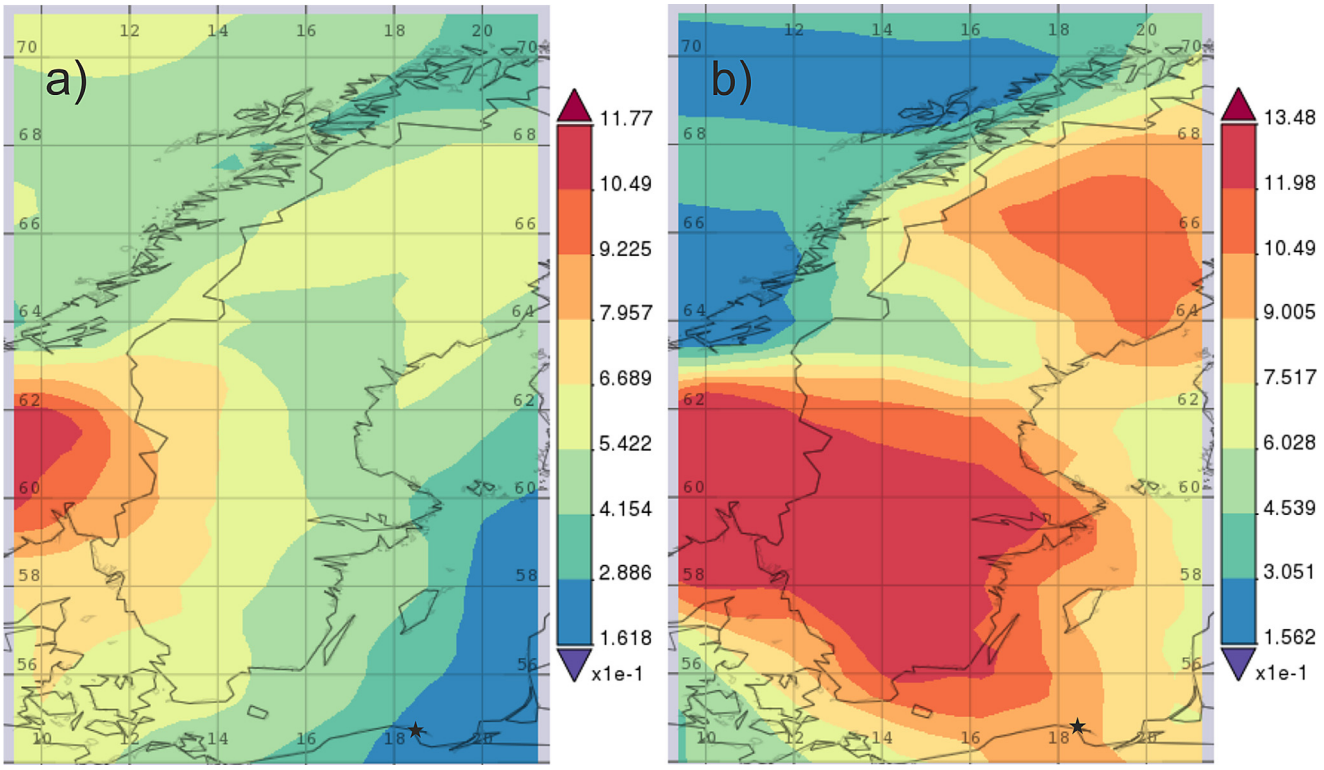

Figure 5 Map of total aerosol Ångstrom parameter (470—870 nm), over 2015-01-08 06Z through 2015-02-08 15Z (a) and 2015-02-09 06Z through 2015-02-09 15Z (b).

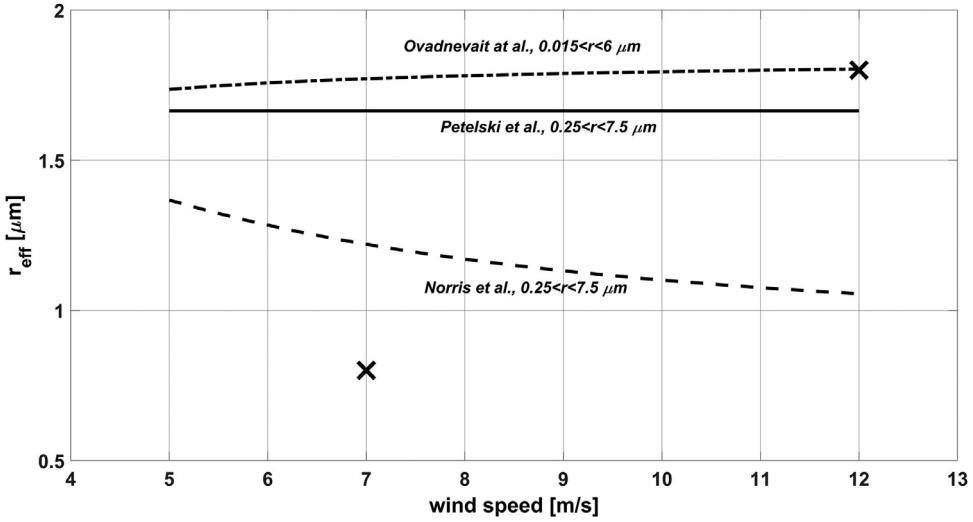

Figure 6 Comparison of theoretical effective radiuses calculated using different SSGF and the values measured at the lowest altitude.

References

Blanchard, D.C., 1954. Bursting of bubbles at an air-water interface. Nature 173 (4413) 1048—1048.

Bodhaine, B.A., Wood, N.B., Dutton, E.G., Slusser, J.R., 1999. On Rayleigh Optical Depth Calculation. J. Atm. Ocean. Tech. 16, 1854—1861.

Bohren, C.F., Huffmann, D.R., 2010. Absorption and scattering of light by small particles. Wiley-Interscience.

Chomka, M., Petelski, T., 1997. Modelling the sea aerosol emission in the coastal zone. Oceanologia 39 (3), 211—225.

Chudzyński, S., Karasiński, G., Skubiszak, W., Stacewicz, T., 2004. Simple polichromator for multi wavelength lidar. SPIE Proc. 5566, 1—4. https://doi.org/10.1117/12.577095

Cipriano, R.J., Blanchard, D.C., Hogan, A.W., Lala, G.G., 1983. On the Production of Aitken Nuclei from Breaking Waves and Their Role in the Atmosphere. J. Atmos. Sci. 40 (2), 469—478.

de Leeuw, G., Andreas, E.L., Anguelova, M.D., Fairall, C.W., Lewis, E.R., O'Dowd, C., Schulz, M., Schwartz, S.E., 2011. Pro-

duction flux of sea spray aerosol. Rev. Geophys. 49, RG2001. https://doi.org/10.1029/2010RG000349

Draxler, R.R., Rolph, G.D., 2010. HYSPLIT (Hybrid Single-particle Lagrangian Integrated Trajectory) Model Access via NOAA ARL READY Website. NOAA Air Resources Laboratory, Silver Spring, MD. http://ready.arl.noaa.gov/HYSPLIT.php

Forster, P., Ramaswamy, V., Artaxo, P., Berntsen, T., Betts, R., Fahey, D.W., Haywood, J., Lean, J., Lowe, D.C., Myhre, G., Nganga, J., Prinn, R., Raga, G., Schulz, M., Van Dorland, R., 2007. Changes in Atmospheric Constituents and in Radiative Forcing. In: Climate Change 2007: The Physical Science Basis. Contribution of Working Group I to the Fourth Assessment Report of the Intergovernmental Panel on Climate Change. [Solomon, S., D. Qin, M. Manning, Z. Chen, M. Marquis, K.B. Averyt, M. Tignor and H.L. Miller (eds.)]. Cambridge Univ. Press, Cambridge UK, New York, USA.

GMAO, 2015. Global Modeling and Assimilation Office (GMAO)m MERRA-2 tavgM_2d_aer_Nx: 2d, Monthly mean, Time-averaged, Signal-Level, Assimilationm Aerosol Diagnostics V5.12.4, Greenbelt, MD, USA, Goddard Earth Sciences Data and Information Services Center (GES DISC), Accessed: 10.5067/FH9A0MLJPC7N.

Jagodnicka, A.K., Stacewicz, T., Karasiński, G., Posyniak, M., Malinowski, S.P., 2009. Particle size distribution retrieval from multiwavelength lidar signals for droplet aerosol. Appl. Optics 48, B8—B16. https://doi.org/10.1364/AO.48.0000B8

Kikas, Ü., Reinart, A., Pugatshova, A., Tamm, E., Ulevicius, V., 2008. Microphysical, chemical and optical aerosol properties in the Baltic Sea region. Atmos. Res. 90, 211—222. https://doi.org/10.1016/j.atmosres.2008.02.009

Kuśmierczyk-Michulec, J., 2009. Ångström coefficient as an indicator of the atmospheric aerosol type for a well-boundry layer: Part 1: Model development. Oceanologia 51 (1), 5—38. https://doi.org/10.5697/oc.51-1.005

Kuśmierczyk-Michulec, J., Marks, R., 2000. The influence of sea-salt aerosols on the atmospheric extinction over the Baltic and North Seas. J. Aerosol Sci. 31 (11), 1299—1316. https://doi.org/10.1016/S0021-8502(00)00032-X

Kuśmierczyk-Michulec, J., Rozwadowska, A., 1999. Seasonal changes of the aerosol optical thickness for the atmosphere over the Baltic Sea-preliminary results. Oceanologia 41 (2), 127—145.

Lewandowska, A.U., Falkowska, L.M., 2013a. Sea salt in aerosols over the southern Baltic. Part 1. The generation and transportation of marine particles. Oceanologia 55 (2), 279—298. https://doi.org/10.5697/oc.55-2.279

Lewandowska, A.U., Falkowska, L.M., 2013b. Sea salt in aerosols over the southern Baltic. Part 2. The neutralizing properties of sea salt and ammonia. Oceanologia 55 (2), 299—318. https://doi.org/10.5697/oc.55-2.299

Lewis, E.R., Schwartz, S.E., 2004. Sea Salt Aerosol Production: Mechanism, Methods, Measurements and Models — A Critical Review. Geophys. Monogr. Ser. 152, 413 AGU, Washington.

Lohmann, U., Feichter, J., 2005. Global Indirect Aerosol Effects: A Review. Atmos. Chem. Phys. 5, 715—737. https://doi.org/10.5194/acp-5-715-2005

Markuszewski, P., Klusek, Z., Nilsson, E.D., Petelski, T., 2020. Observations on relations between marine aerosol fluxes and surface-generated noise in the southern Baltic Sea. Oceanologia 62 (4), 413—427. https://doi.org/10.1016/j.oceano.2020.05.001

Massel, S.R., 2007. Ocean Waves Breaking And Marine Aerosol Fluxes. Atmospheric And Ocenaographic Sciences Library. https://doi.org/10.1017/Cbo9781107415324.004

Nadstazik, A., Marks, R., Schulz, M., 2000. Nitrogen species and macroelements in aerosols over the southern Baltic Sea. Oceanologia 42 (4), 411—424.

Norris, S.J., Brooks, I.M., Hill, M.K., Brooks, B.J., Smith, M.H., Sproson, D.A.J., 2012. Eddy covariance measurements of the sea spray aerosol flux over the open ocean. J. Geophys. Res. 117, D07210. https://doi.org/10.1029/2011JD016549

Ovadnevaite, J., de Leeuw, G., Ceburnis, D., Monahan, C., Partanen, A.I., Korhonen, H., O'Dowd, C.D., 2014. A sea spray aerosol flux parameterization encapsulating wave state. Atmos. Chem. Phys. 14 (4), 1837. https://doi.org/10.5194/acp-14-1837-2014

Petelski, T., Chomka, M., 1996. Marine aerosol fluxes in the coastal zone — BAEX experimental data. Oceanologia 38 (4), 469—484.

Petelski, T., Chomka, M., 2000. Sea salt emission in the coastal zone. Oceanologia 42 (4), 399—410.

Petelski, T., Markuszewski, P., Makuch, P., Jankowski, A., Rozwadowska, A., 2014. Studies of vertical coarse aerosol fluxes in the boundary layer over the Baltic Sea. Oceanologia 56 (4), 697—710. https://doi.org/10.5697/oc.56-4.697

Petelski, T., Piskozub, J., Paplinska-Swerpel, B., 2005. Sea spray emission from the surface of the open Baltic Sea. J. Geophys. Res.-Oceans 110 (C10), C10023. https://doi.org/10.1029/2004JC002800

Petelski, T., 2003. Marine aerosol fluxes over open sea calculated from vertical concentration gradients. J. Aerosol Sci. 34 (3), 359—371. https://doi.org/10.1016/S0021-8502(02)00189-1

Plauškaitė, K., Špirkauskaitė, N., Byčenkienė, S., Kecorius, S., Jasinevičienė, D., Petelski, T., Zielinski, T., Andriejauskienė, J., Barisevičiūtė, R., Garbaras, A., Makuch, P., Duboitis, V., Ulevicius, V., 2017. Characterization of aerosol particles over the southern and South-Eastern Baltic Sea. Mar. Chem. 190, 13—27. https://doi.org/10.1016/j.marchem.2017.01.003

Posyniak, M., Malinowski, S.P., Stacewicz, T., Markowicz, K.M., Zieliński, T., Petelski, T., Makuch, P., 2011. Multiwavelength micropulse lidar in atmospheric aerosol study — signal processing. Proc. SPIE 8182, 818216—818226.

Posyniak, M., Stacewicz, T., Miernecki, M., Jagodnicka, A.K., Malinowski, S.P., 2010. Multiwavelength micropulse lidar for atmospheric aerosol investigation. Opt. Appl. 40 (3), 601—608.

Resch, F.J., Darrozes, S.J., Afeti, G.M., 1986. Marine liquid aerosol production from bursting of air bubbles. J. Geophys. Res. 91, 1019—1029. https://doi.org/10.1029/JC091iC01p01019

Seinfeld, J.H., Pandis, S.N., 1997. Atmospheric Chemistry and Physics. John Wiley & Sons, New York.

Sitarek, S., Stacewicz, T., Posyniak, M., 2016. Software for retrieval of aerosol particle size distribution from multiwavelength lidar signals. Comput. Phys. Commun. 199, 53—60. https://doi.org/10.1016/j.cpc.2015.08.024

Spiel, D.E., 1997a. A hypothesis concerning the peak in film drop production as function of bubble size. J. Geophys. Res. 102 (C1), 1153—1161. https://doi.org/10.1029/96JC03069

Spiel, D.E., 1997b. More on the birth jet drops from bubbles bursting on seawater surface. J. Geophys. Res. 102 (C3), 5815—5821. https://doi.org/10.1029/96JC03582

Spiel, D.E., 1998. On the birth film drops from bubbles bursting on seawater surface. J. Geophys. Res. 103 (C11), 24907—24918. https://doi.org/10.1029/98JC02233

Spiel, D.E., 1995. On the birth jet drops from bubbles bursting on seawater surface. J. Geophys. Res. 100 (C3), 4995—5006. https://doi.org/10.1029/94JC03055

Spiel, D.E., 1994. The number and size of jet drops produced by air bubbles bursting at a water surface. J. Geophys. Res. 99 (C5), 10289—10296. https://doi.org/10.1029/94JC00382

Stelmaszczyk, K., Dell'Aglio, M., Chudzyński, S., Stacewicz, T., Wöste, L., 2005. Analytical function for lidar geometrical compression form-factor calculations. Appl. Optics 44 (7), 1323—1331. https://doi.org/10.1364/AO.44.001323

Stevens, B., Feingold, G., 2009. Untangling aerosol effects on clouds and precipitation in a buffered system. Nature 461, 607—613. https://doi.org/10.1038/nature08281

Streets, D.G., Wu, Y., Chin, M., 2006. Two-Decadal Aerosol Trends as A Likely Explanation of The Global Dimming/Brightening Tran-

sition. Geophys. Res. Lett. 33 (15), L15806. https://doi.org/10.1029/2006GL026471

Tao, W.K., Chen, J.P., Li, Z., Wang, C., Zhang, C., 2012. Impact of aerosols on convective clouds and precipitation. Rev. Geophys. 50, RG2001. https://doi.org/10.1029/2011RG000369

Twomey, S., 1977. The Influence of Pollution on the Shortwave Albedo of Clouds. J. Atmos. Sci. 34, 1149—1152. https://doi.org/10.1175/1520-0469(1977)034⟨1149:TIOPOT⟩2.0.CO;2

Wood, R., Wyant, M., Bretherton, Ch.S., Rémillard, J., Kollias, P., Fletcher, J., Stemmler, J., de Szoeke, S., Yuter, S., Miller, M., Mechem, D., Tselioudis, G., Chiu, J.Ch., Mann, J.A.L., O'Connor, E.J., Hogan, R.J., Dong, X, Miller, M., Ghate, V., Jefferson, A., Min, Q., Minnis, P., Palikonda, R., Albrecht, B., Luke, E., Hannay, C., Lin, Y., 2015. Clouds, aerosol, and precipitation in the marine boundary layer: An ARM mobile facility deployment. B. Am. Meteorol. Soc. 96, 419—440. https://doi.org/10.1175/BAMS-D-13-00180.1.

Zdun, A., Rozwadowska, A., Kratzer, S., 2011. Seasonal variability in the optical properties of Baltic aerosols. Oceanologia 53 (1), 7—34. https://doi.org/10.5697/oc.53-1.007

Zdun, A., Rozwadowska, A., Kratzer, S., 2016. The impact of air mass advection on aerosol optical properties over Gotland (Baltic Sea). Atmos. Res. 182, 142—155. https://doi.org/10.1016/j.atmosres.2016.07.022

Zieliński, T., 2004. Studies of aerosol physical properties in coastal areas. Aerosol Sci. Tech. 38 (5), 513—524. https://doi.org/10.1080/02786820490466738